An NMR Study of a 300-kDa AAA+ Unfoldase

Georg Krüger [1], **John Kirkpatrick** [2], **Emilie Mahieu** [3], **Bruno Franzetti** [3], **Frank Gabel** [3] **and Teresa Carlomagno** [1,2,4]*

1 - Centre of Biomolecular Drug Research and Institute of Organic Chemistry, Leibniz University Hannover, Schneiderberg 38, 30167 Hannover, Germany

2 - School of Biosciences, College of Life and Environmental Sciences, University of Birmingham, Edgbaston, Birmingham B15 2TT, UK

3 - Univ. Grenoble Alpes, CEA, CNRS, IBS, 71 avenue des Martyrs, F-38000 Grenoble, France

4 - Institute of Cancer and Genomic Sciences, College of Medical and Dental Sciences, University of Birmingham, Edgbaston, Birmingham B15 2TT, UK

Correspondence to Teresa Carlomagno:*School of Biosciences, College of Life and Environmental Sciences, University of Birmingham, Edgbaston, Birmingham B15 2TT, UK   *t.carlomagno@bham.ac.uk* (T. Carlomagno) *@CarlomagnoNMR* 🐦 (T. Carlomagno)
https://doi.org/10.1016/j.jmb.2023.167997
Edited by M.F. Summers

Abstract

AAA+ ATPases are ubiquitous hexameric unfoldases acting in cellular protein quality control. In complex with proteases, they form protein degradation machinery (the proteasome) in both archaea and eukaryotes. Here, we use solution-state NMR spectroscopy to determine the symmetry properties of the archaeal PAN AAA+ unfoldase and gain insights into its functional mechanism. PAN consists of three folded domains: the coiled-coil (CC), OB and ATPase domains. We find that full-length PAN assembles into a hexamer with C_2 symmetry, and that this symmetry extends over the CC, OB and ATPase domains. The NMR data, collected in the absence of substrate, are incompatible with the spiral staircase structure observed in electron-microscopy studies of archaeal PAN in the presence of substrate and in electron-microscopy studies of eukaryotic unfoldases both in the presence and in the absence of substrate. Based on the C_2 symmetry revealed by NMR spectroscopy in solution, we propose that archaeal ATPases are flexible enzymes, which can adopt distinct conformations in different conditions. This study reaffirms the importance of studying dynamic systems in solution.

Introduction

AAA+ (ATPases associated with diverse cellular activities) unfoldases are essential components of protein quality control mechanisms in all three domains of life[1]: together with chaperones, they dissemble and refold protein aggregates; together with proteases they degrade misfolded or superfluous proteins.[2,1] In eukaryotes, archaea and some bacteria, proteolytic machinery consists mostly of AAA+ unfoldase and protease complexes called proteasomes.[4] The 26S eukaryotic proteasome, for example, is composed of a 20S proteolytic core particle (CP) and a 19S AAA+ ATPase regulatory particle (RP),[5] which consists of a hetero-hexameric AAA+ unfoldase, comprising the proteins Rpt_{1-6}, and 13 accessory proteins.[6] Eukaryotic protein degradation requires the

ubiquitin-processing activity of the RP accessory proteins, as ubiquitylation marks the proteins destined for degradation. The architecture of the archaeal proteasome is simpler[7]: the RP is an homo-hexamer of the proteasome-activating nucleotidase protein (PAN) and the 13 accessory proteins are apparently missing. In archaea, the question of how substrates are recruited to the proteolytic machinery is still open: proteins destined for degradation may be sampylated (covalently labelled with small archaeal ubiquitin-like modifier proteins (SAMPs)),[8] but other degradation signals, such as flexible and unstructured tails, are functional in vitro[9] and may also be relevant in vivo.

The eukaryotic protomers Rpt$_{1-6}$ and archaeal PAN share a common domain architecture consisting of an N-terminal coiled-coil (CC) domain, an oligosaccharide-/oligonucleotide-binding (OB) domain and an ATPase domain (Figure 1 (A)). The CC domains of pairs of neighbouring subunits form three coiled-coil structures per unfoldase hexamer. In the eukaryotic 19S RP, the CC domain structures are involved in binding to the accessory proteins, but in archaea their function, as well as that of the unfolded tails located N-terminal to the CC domains, is not fully understood.

Based on several cryo-electron-microscopy (cryo-EM) structures of proteolytic machinery with and without substrate,[2,10–17] a sequential mechanism for unfolding and translocation to the protease chamber has been proposed, whereby the substrate is handed over from one unfoldase subunit to the other (hand-over-hand); contemporarily, the unfoldase subunits cycle clockwise through a spiral staircase arrangement, using energy from ATP hydrolysis. In this model, the six OB domains of the AAA+ unfoldase subcomplex form a flat ring, while five of the six ATPase domains form the staircase. The lowest-positioned ATPase domain (that closest to the CP) is either bound to ADP or devoid of any nucleotide and is disengaged from the staircase. Of the five ATPase domains in the staircase, the lowest is bound to ADP, while the other four contain ATP (Figure S1). In the absence of substrate the staircase is steeply pitched, but becomes flattened during substrate processing.[10] When the disengaged ATPase domain binds ATP, the second-lowest member of the staircase hydrolyses ATP, to maintain four ATP copies per ring. These two events induce conformational changes, which cause the previously disengaged ATPase domain to move to the top-position of the staircase and the previously lowest member of the staircase to disengage. In this way, the ATPase ring "rotates" clockwise (looking from the opposite side to that bound by the CP) by one unit and the substrate is translocated to the protease chamber by two amino acids per molecule of hydrolysed ATP. In the only cryo-EM structure of an archaeal proteasome,[17] the movement of the ATPase domains appears to be correlated with the engagement of the pore-facing loops with the substrate, linking the ring "rotation" with substrate translocation. Finally, the similarity of this structure and the cryo-EM structures of the bacterial proteolytic complex ClpXP (consisting of the hexameric unfoldase ClpX and the protease ClpP) to the structure of eukaryotic proteasomes[18–20] supports a similar translocation mechanism for all three kingdoms of life.

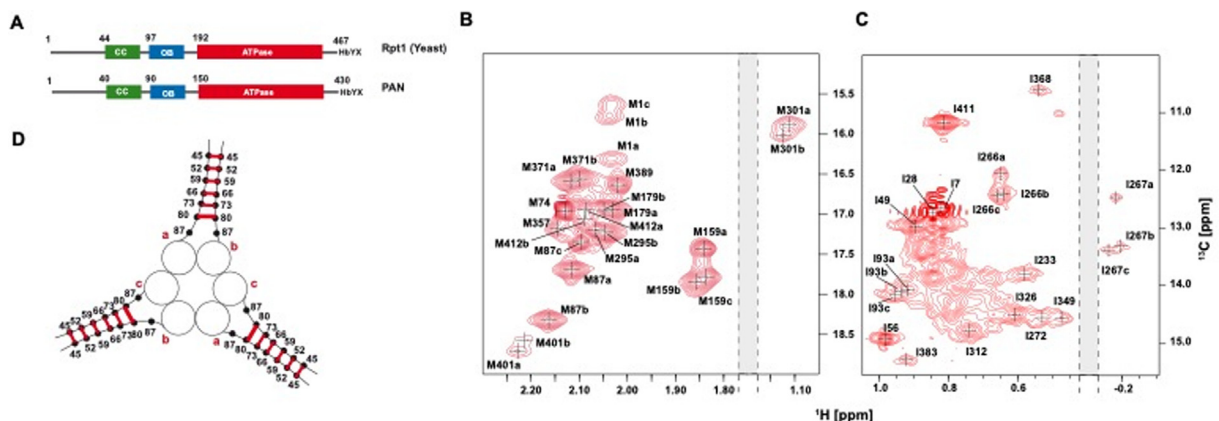The hand-over-hand translocation mechanism has been challenged by single-molecule studies of

Figure 1. PAN has a C$_2$ symmetry. (A) The domain architecture of proteasomal ATPases from yeast (S. cerevisiae Rpt1) and archaea (M. jannaschii PAN). Three of the six protomers in Rpt1 and all six protomers in PAN carry a C-terminal HbYX amino-acid motif (hydrophobic-tyrosine-any), which interacts with the core particle. (B) and (C) ^{1}H,^{13}C-HMQC spectra of selectively ^{1}H,^{13}C-labelled Met-ε and Ile-δ1 perdeuterated PAN (20 μM hexamer) in the presence of 50 mM ADP. For several residues, we could identify up to three distinct peaks. (D) Schematics of the CC domains. a, b and c indicate three different conformations at the C-terminal end of the CC helix, which result in three peaks for M87 and in C$_2$ symmetry. Along the CC helix, amino acids are shown in groups of seven, as a heptad is the minimal subunit of the CC structure.

ClpXP, which used optical-trapping nanometry to demonstrate that translocation does not occur sequentially but rather in bursts, with a stochastic distribution of the translocation step-size around an average of 5–8 amino acids.[21–24] These findings, together with the fact that the activity of ClpXP assembled with as many as four mutant unfoldase subunits incapable of ATP hydrolysis is still signifi-

cant,[25] led the authors to conclude that translocation occurs stochastically rather than sequentially.

In the cryo-EM structures, 5–6 copies of the unfoldase protomer are in the nucleotide-bound state. This stoichiometry appears to conflict with biochemical studies reporting that a maximum of four nucleotide molecules bind simultaneously to the unfoldase hexameric ring,[26,27] which contains
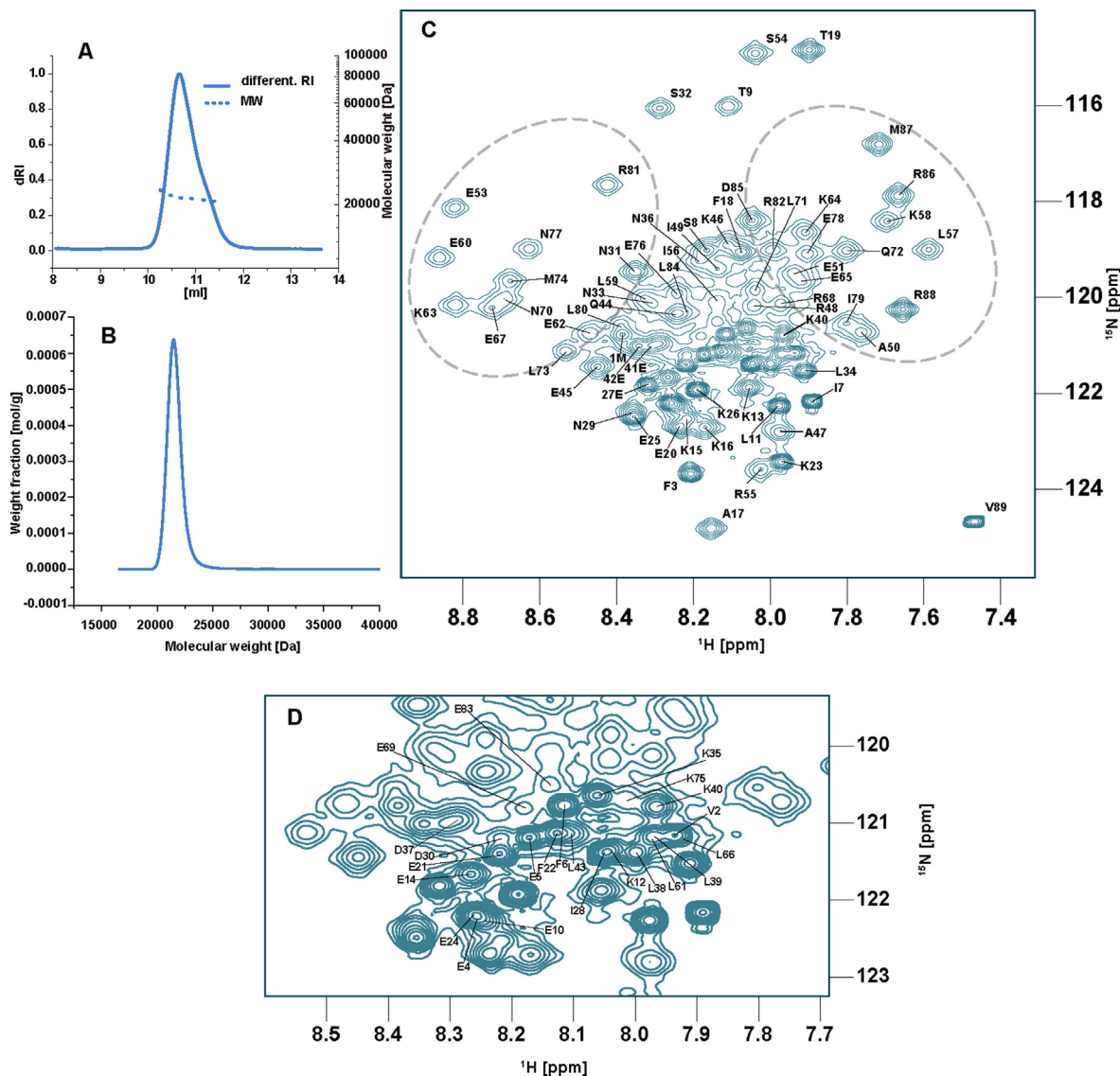

Figure 2. The PAN coiled-coil domain forms a homodimer. (A, B) SEC-MALS analysis of the isolated coiled-coil domain (PAN$^{1-89}$), which forms a 21.75-kDa dimer. Panel A shows the differential refractive index (dRI) value (left vertical axis, solid line, relative scale from 0 to 1) and the measured molecular-weight (right vertical axis, dashed line) of the SEC elution. Panel B shows the distribution of molecular weights over the eluted sample. (C) ^{1}H,^{15}N-HSQC spectrum of PAN$^{1-89}$: ~30 peaks are sharp and intense, indicating the presence of an unfolded stretch, while ~40 other peaks correspond to a region of PAN$^{1-89}$ adopting a well-defined secondary structure (some of these well-dispersed peaks are encircled). The peaks are labelled with the residue-specific assignments. Only one amide peak was observed for each residue, indicating a symmetric arrangement of the two protomers. D). Excerpt of the ^{1}H,^{15}N-HSQC spectrum of C) showing peak assignments in the most crowded region. Assignment spectra were recorded at 45 °C on a 600 MHz spectrometer. Samples contained 500–1000 μM monomeric PAN$^{1-89}$.

three types of ATP binding-sites with distinct affinities for the nucleotide. In PAN, two protomer sites bind ATPγS with a dissociation constant K_D of 0.5 µM, two sites with a K_D of 113 µM and the other two sites with only very weak affinity. Furthermore, optimal substrate binding to the unfoldase was achieved at ATP concentrations that support binding of only two ATP molecules.[26] Similar results were also reported for eukaryotic and bacterial AAA+ unfoldases.[28] On the other hand, a recent native mass spectrometry study found that six nucleotide molecules are stably bound to one PAN hexamer.[29] Thus, the exact stoichiometry of ATP-binding by PAN remains unclear.

Here we use solution nuclear magnetic resonance (NMR) spectroscopy to study the architecture of AAA+ unfoldases in solution and determine whether it endorses the spiral staircase model. For these investigations, we have used PAN from the thermophilic archaeon *Methanocaldococcus jannaschii* (*Mj*). Unfoldases from thermophilic organisms are well-suited for NMR studies as the quality of the spectra of large complexes improves at high temperatures.[30,31] We find that in solution, in the presence of nucleotide but in the absence of substrate, PAN has a C_2 symmetry, with the C_2 axis likely going through the center of the ring. The symmetry extends from the C-terminal end of the CC domains through the OB domains to the ATPase domains. This symmetry is difficult to reconcile with the spiral staircase model but fits well with the existence of three sets of pairwise-similar nucleotide binding pockets. The CC and OB domains do not appear to recruit the substrate but rather contribute to determining the overall PAN architecture. In light of our data, we propose that archaeal PAN does not adopt a staircase architecture in the absence of substrate but rather a pre-catalytic, resting state with C_2 symmetry that recapitulates the nucleotide binding properties measured in biochemical experiments. The staircase architecture would then be induced by substrate recruitment, which could be the factor underlining the higher ATPase activity of the machinery in the presence of substrate. This work reiterates the importance of NMR spectroscopy for the study of dynamic complexes, even those of very large size.

Results

The NMR spectra of PAN sub-domains. First, we assigned the NMR resonances of the individual CC (PAN$^{1-89}$), OB (PAN$^{74-150}$) and ATPase (PAN$^{150-430}$) domains of the *Mj* PAN with standard NMR experiments.

PAN$^{1-89}$ formed a dimer in solution (Figure 2). Only one set of peaks was present in all spectra, indicating that the dimer is symmetric. Backbone assignment was obtained to completeness (except for residue E51, whose peaks were

missing from the spectra). The first 40 residues were disordered, as indicated by both secondary chemical shifts and relaxation data (Figure S2). Residues 40–88 formed a long helix, with a possible kink at the position of E51.

PAN$^{74-150}$ formed a hexamer in solution (Figure 3 (D)). Backbone assignment covered the majority of PAN$^{74-150}$ with the exception of stretches 74–78 and 111–114 (Figure 3(E)). We observed up to six distinct peaks per residue in the ^{1}H,^{15}N-HSQC spectrum (Figure 3(E) and (F)). For some residues, such as T143, the six peaks were all localized in the same spectral region (Figure 3(A) and (B)), while for some others, such as L142, the six peaks clustered into two sets appearing in different spectral regions (Figure 3(A) and (C)). Overall, the NMR spectra suggested a complete lack of symmetry in the hexamer. By contrast, the crystal structure of the *Mj* PAN OB domain[32] is a trimer of asymmetric dimers (C_3 symmetry), containing two types of protomers differing in the configuration of the peptide bond between P90 and P91, where an alternating *cis* and *trans* configuration allows for the formation of CC dimers and positions the dimer on the top of the OB domain contributing P91 in *cis* (Figure 3(G)). In the crystal structure, all other residues of the OB fold have the same conformation.

Wild-type PAN$^{150-430}$ formed a mixture of oligomers containing one to six protomers per complex (Figure S3), leading to NMR spectra of poor quality. Thus, we generated the mutant F196A, which according to previous literature reports[33] weakens inter-protomer interactions. The F196A PAN$^{150-430}$ mutant was a stable monomer in solution, allowing for the assignment of >94% of the backbone resonances (Figure S3).

The symmetry of the PAN hexamer. First, we sought to determine the architecture of full-length (FL) PAN by monitoring the NMR resonances of the 282-kDa hexameric ring in solution. To obtain a monodisperse hexameric complex, we tested several buffer conditions, varying salt and nucleotide concentrations: the best-quality NMR spectra were obtained for 120 µM PAN monomer assembled into 20 µM hexameric PAN in 50 mM ATP or ADP, 20 mM Tris-HCl, 100 mM NaCl, 10 mM MgCl$_2$, pH* 7.1 (pD 7.5), 100 % D$_2$O. In the absence of nucleotide, PAN existed as a mixture of hexamers and dodecamers (Figure S4). The proportion of dodecamers could be decreased in high-salt buffers (500 mM NaCl), but good-quality NMR spectra of active PAN were obtained only in the presence of either ADP or ATP.

In this molecular-weight range, solution NMR relies heavily on the selective observation of methyl-group resonances in ^{1}H,^{13}C-HMQC spectra of uniformly deuterated, ^{1}H,^{13}C-methyl labelled proteins. Methyl-group resonances have favorable relaxation properties and yield peaks with strong signal intensity.[31,34] Because of exten-
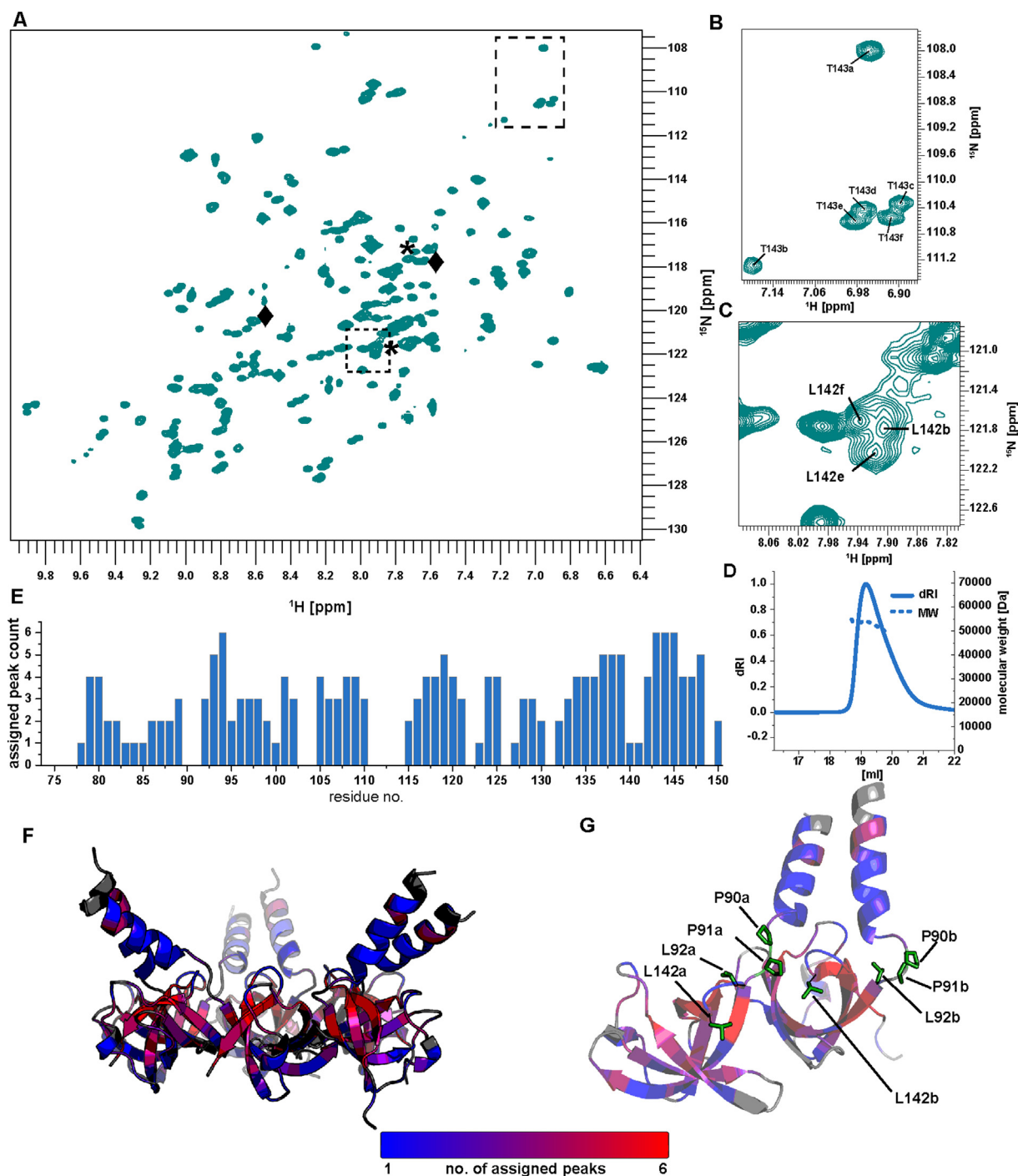
Figure 3. The PAN OB domain forms a hexameric complex. (A) ^{1}H,^{15}N-TROSY spectrum of PAN$^{74–150}$. The presence of 216 resolvable peaks reveals that PAN$^{74–150}$ exists in several different conformations. Sequential assignment yielded up to six peaks per residue. Diamonds and asterisks indicate the peak clusters corresponding to distinct conformations of L92 and L142, for which the three and four peaks, respectively, are located in very different regions of the spectrum. (B) and (C) Excerpts of the spectrum shown in A in dashed rectangles. (D) SEC-MALS analysis of PAN$^{74–150}$, showing that the domain forms a hexamer of ∼54 kDa. The dRI is reported on a relative scale from 0 to 1. The six conformations seen in (A) are likely to correspond to different conformations of the protomer in the hexameric complex. (E) Number of conformations identified and assigned for each residue. (F) Number of conformations assigned for each residue color-coded on the X-ray structure of PAN$^{74–150}$ OB domain (PDB entry 3H43). (G) Close-up of the structure in (F) highlighting the two different geometries of the P90–P91 amide bond (*cis* and *trans*) of the pair of neighbouring protomers whose N-terminal helices interact to form the coiled-coil structure. All spectra were recorded at 60 °C on an 850 MHz spectrometer with perdeuterated, ^{15}N,^{13}C-labelled PAN$^{74–150}$ at 600 μM (monomer concentration).

sive resonance overlap in the leucine and valine methyl-group region, we focused our attention on the methyl groups of isoleucine and methionine in selectively IM-labelled samples (Figure 1(B) and (C)). From the previous partial assignment of the side-chains of individual domains, we could make assignments for the two Ile-δ1 methyl-groups of the OB domain of FL PAN (I79 and I93), as well as for all nine Met-ϵ and 10 out of 22 Ile-δ1 methyl-groups of the ATPase domain (Figure 4 (A)–(D)). The methyl-groups of an additional six residues in the CC domain were assigned by point mutations (I7, I28, I49, I56, M74 and M87, Figure 4 (E)). Additional point mutations (M179, M295 and M412) were used to confirm assignments.

The ^{1}H,^{13}C-HMQC spectrum of IM-labelled FL PAN showed between one and three peaks per residue (Figure 1(B) and (C)). Three resolvable peaks were seen for M1, M87, I93, M159, I266 and I267, spanning all three domains. In these cases, the peaks had approximately equal volumes, suggesting that the structure of the PAN hexamer has C_2 symmetry. Residues M295, M301, I368, M371, M401 and M412 (and possibly M179) appeared to show two peaks. When we performed peak integration using the line-shape fitting program FuDA (D.F. Hansen, https://www.ucl.ac.uk/hansen-lab/fuda/), we measured a volume-ratio of $\sim$2:1 for the two peaks of M295, M301, I368 and M401, which is compatible with a C_2-symmetric structure of the hexamer, assuming that the resonances of two of the three protomer structures have similar chemical shifts. In contrast, the volumes of the two peaks of M371 and M412 were similar, apparently contradicting the presence of three conformations. However, for these two amino acids the presence of a third peak cannot be excluded because of spectral crowding. Careful analysis of all the wild-type and mutant spectra revealed two additional peaks partially overlapped with those of M412, which did not disappear in the spectrum of the M412A mutant. One of these two peaks could represent the third conformation of M371, while both additional peaks distort the apparent volume-ratio of the two peaks assigned to M412, making their relative intensity appear approximately equal. For all other residues, we could not unambiguously determine the number of peaks due to spectral crowding. However, more than three conformations were not observed for any residue. These results establish that in solution, in the presence of nucleotide but in the absence of substrate, archaeal PAN adopts a structure with C_2 symmetry, with the symmetry axis likely going through the centre of the ring (Figure 1(D)).

In the presence of 50 mM ATP, the ^{1}H,^{13}C-HMQC spectrum of FL PAN was identical to that recorded in the presence of ADP, indicating that the symmetry of PAN is the same when bound to either ADP or ATP. The post-measurement ADP:

ATP ratio was $\sim$60:40, confirming that enough ATP to saturate all PAN binding sites ($\leq$120 μM) was present throughout the acquisition of the NMR spectra.

To verify that the PAN construct described above is catalytically active, we tested its activity using GFP as substrate (Figure 5(A)). We chose GFP because its high melting-temperature (>80 °C)[35] makes it suitable for catalytic unfolding studies at 50–60 °C; in addition, its intrinsic fluorescence provides an additional means of monitoring the unfolding reaction. The GFP carried a bacterial ssrA-tag at its C-terminus for targeting to the unfoldase.[36] 5 μM FL PAN, either alone or in combination with equimolar quantities of the 20S proteolytic CP, unfolded 100 μM GFP at 60 °C. The overall rate of unfolding increased in the presence of the 20S CP, confirming that the 20S particle has an activating effect on PAN, as described previously.[37]

Next, we asked whether the C_2 symmetry seen in the NMR spectra of IM-labelled PAN could be reconciled with the existing cryo-EM structures. To answer this question, we inspected the position of residues in the cryo-EM structures of the archaeal proteasome from *Archaeoglobus fulgidus* (*Af*) that correspond to those with well-resolved methyl-groups in the NMR spectra of IM-labelled *Mj* PAN.[17] In the presence of substrate, the *Af* PAN–proteasome complex was found in five conformational states, differing in the offset of individual PAN protomers from the cognate surface of the proteasome. We inspected the environment of the side-chains of the residues of *Af* PAN corresponding to M87, I93, M159, I266, I267, M295, M301, I368, M371, M401 and M412 in *Mj* PAN in the six PAN protomers of all five *Af* PAN conformations. We refrained from building and inspecting structural models of the *Mj* PAN generated using the structures of *Af* PAN as templates, because of the low-resolution of the EM structures of *Af* PAN (6.5–7.5 Å for the entire structure and 4.85 Å in the ATPase ring)[17] and the expected lack of accuracy in the prediction of the conformations of the side-chains of *Mj* PAN. Thus, our analysis focused on identifying substantial differences in the environment of the NMR-visible side-chains in the six subunits, rather than revealing subtle conformational variations.

Firstly, the presence of three conformations for M87 and I93 is not predicted by the cryo-EM conformers. *Mj* I93 is at the N-terminal end of the OB domain and the corresponding residue in the cryo-EM structure of *Af* PAN, L64, faces β-strand β3 of the neighbouring protomer (Figure 6(A)). The distance to the closest residue of the neighbouring sub-unit, F87, is similar across all interfaces, except for one, where F87 is tilted away from L64 (green and blue in Figure 6(A), respectively). *Mj* M87 corresponds to *Af* L58, which is located three residues before the ^{61}PP^{62} dyad whose conserved P62 residue was found to
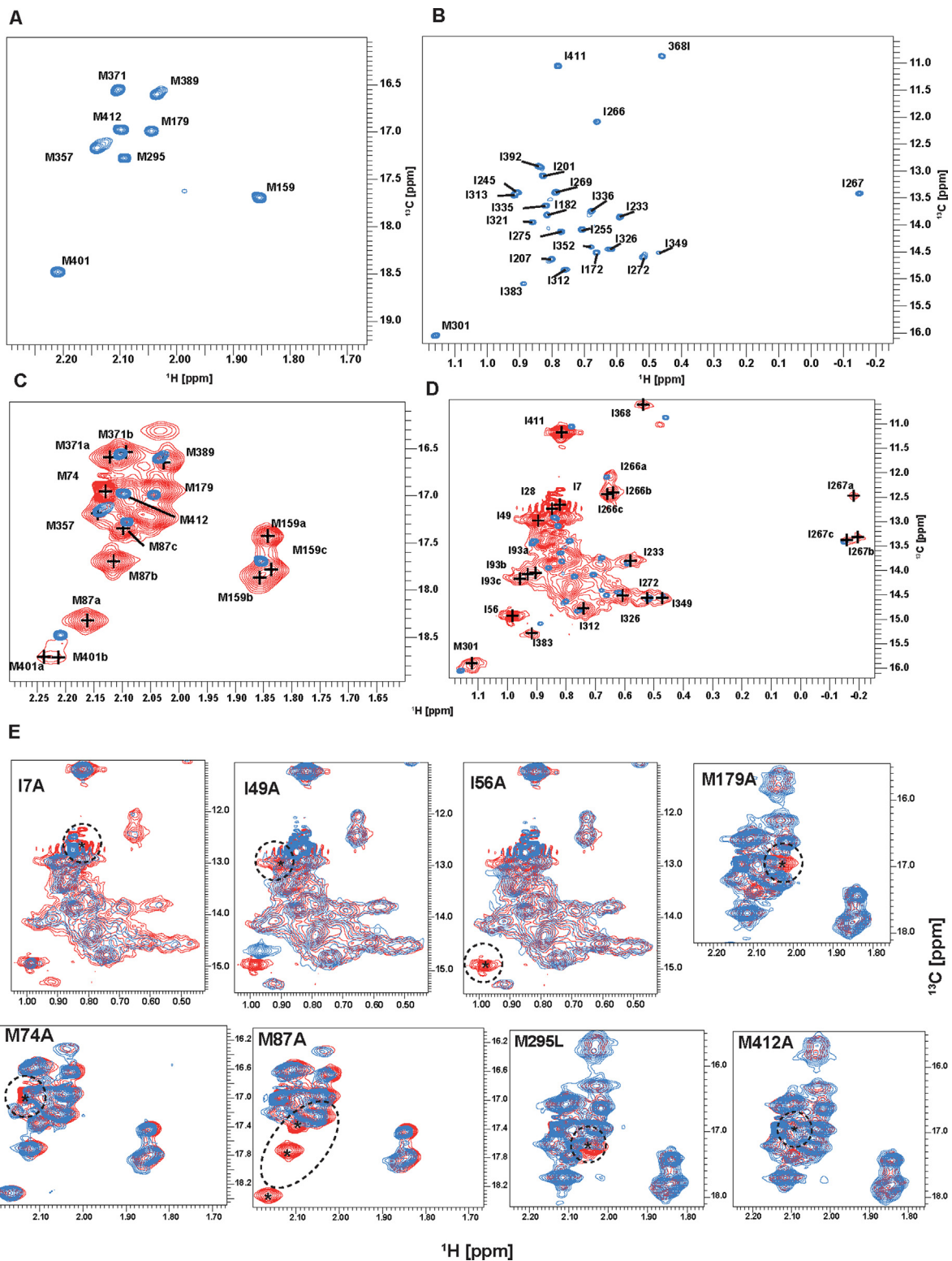
Figure 4. Resonance assignment strategy for the methyl groups of full-length PAN. (A) and (B) ^{1}H,^{13}C-HMQC spectrum of mutant PAN$^{150–430}$F196A with methionine-ε (A) and isoleucine-δ1 (B) methyl-group resonance assignments. (C) and (D) Overlay of the mutant PAN$^{150–430}$F196A ^{1}H,^{13}C-HMQC spectrum (blue) with the FL PAN ^{1}H,^{13}C-HMQC spectrum (red). The methionine-ε and isoleucine-δ1 regions are shown in (C) and (D), respectively. Assigned peaks are labelled. (E) Overlays of the ^{1}H,^{13}C-HMQC spectrum of wild-type FL PAN (red) with those of several point mutants (blue). The encircled asterisks indicate peaks which disappear in the mutant spectra. All spectra were recorded on 20 μM PAN hexamer in 100% D$_2$O-based buffers at 60 °C on an 850 MHz spectrometer.
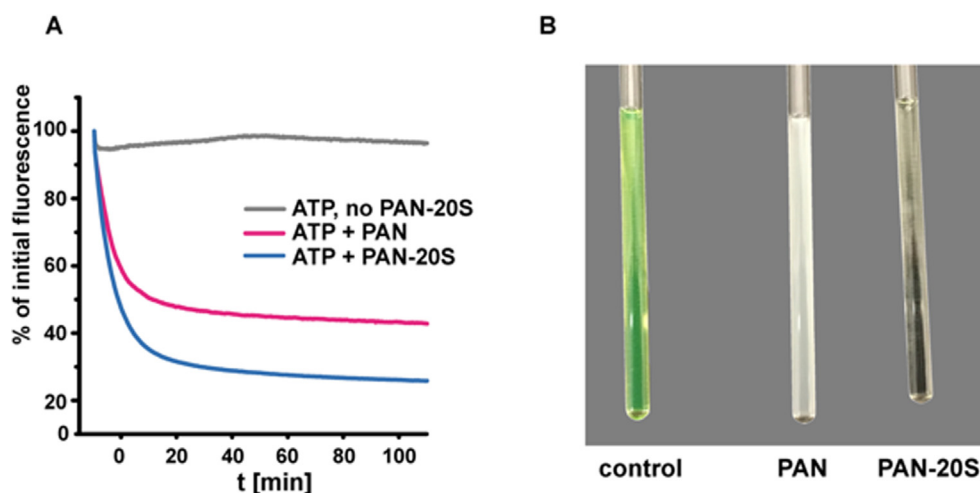
Figure 5. GFP-ssrA is a substrate of both PAN and PAN–20S. (A) Fluorescence decays of GFP-ssrA (100 μM) at 60 °C in the presence of either PAN (5 μM, pink) or PAN–20S (5 μM, blue), with 100 mM ATP and 100 mM MgCl$_2$. The control reaction (without PAN and the 20S CP) is in grey. The decays can be fitted by a biexponential function. The values of the shorter time-constant T_1 are $T_{1, unfolding} = 341 \pm 12$ s (with PAN) and $T_{1, proteolysis} = 243 \pm 44$ s (with PAN–20S). Fluorescence measurements were carried out in triplicate and the uncertainty corresponds to the standard error of the mean of the three fitted time-constants. (B) NMR tubes containing the same reaction-mix as in (A) after incubation at 60 °C for 3 h. The addition of PAN results in the formation of white precipitate, while the addition of PAN–20S leads to a clear, colorless solution.

alternate between the *trans* and *cis* geometries, thereby positioning the coiled-coil domains above the OB domains of the subunits with P62 in the *cis* geometry.[38] This residue shows three distinct peaks in the ^{1}H,^{13}C-HMQC spectrum, contradicting the C$_3$ symmetry arising from alternating P62 *cis/trans* geometries and suggesting instead three different orientations of the coiled-coil domains with respect to the OB ring (Figure 1(D)). In the cryo-EM study of *Af* PAN, the coiled-coil domains were found to be flexible. Nevertheless, in all structures the positions of the three L58 residues preceding the P62 residues with *cis* geometry are similar: L58 is sandwiched between the L58 and the flexible R59 residues of the neighbouring protomer (Figure 6(B)–(D)). Similarly, all three L58 residues preceding the P62 residues with *trans* geometry are sandwiched between the L58 and the R59 residues of the neighbouring protomer, with R59 being held in place by a salt-bridge with the S92 residue of the β3–β4 loop (Figure 6(C)). Notwithstanding the low resolution of the cryo-EM structures, which impinges on the reliability of the side-chain conformations, the C$_2$ symmetry seen for M87 and I93 in the NMR spectrum of the PAN homohexamer is not reproduced in the cryo-EM conformers.

Secondly, we considered the residues *Mj* M159 and M295: these correspond to *Af* F130 and M266, and are critical indicators of the arrangement of the PAN protomers in the hexamer, being at the interface between two ATPase subunits. In the NMR spectrum, *Mj* M159 shows three distinct peaks with approximately equal volumes. In the cryo-EM structures, the corresponding residue *Af* F130 is found in four different environments. F130 of the disengaged (lowest) protomer contacts M266 in helix α6 of the highest subunit (Figure 7(A)). F130 of the second-lowest subunit (lowest in the spiral staircase) is close to helix α5 of the disengaged subunit and may contact R224 (Figure 7(B)). In the following protomers, F130 is either juxtaposed to helix α5 of the neighbouring subunit (Figure 7(F)) or projected towards helix α5 of the same subunit (Figure 7(C) and (E)), or contacts the OB domain of the neighbouring subunit (Figure 7(D)). For this residue, none of the five structures of *Af* PAN reproduces the C$_2$ symmetry revealed in the NMR spectra. *Af* M266 is located on helix α6 one turn below the portion of the helix that builds the nucleotide binding pocket. The corresponding residue *Mj* M295 shows two peaks in the NMR spectrum with a volume-ratio of 2:1. Again, the cryo-EM structures do not reproduce the C$_2$ symmetry seen in the NMR spectrum. While the environment of *Af* M266 is very similar in four of the six protomers, with M266 contacting E242 and D244 of the α6–β9 loop of the neighbouring protomer (Figure 7(H)–(K)), the environments of the other two protomers are quite different from the first four and from each other. At the interface between the lowest and second-lowest protomers, M266 is juxtaposed to the same loop but the interface is quite loose (Figure 7(G)). Finally, at the interface between the lowest and highest protomers, M266 contacts F130 in the long loop that connects the OB and the ATPase domains (Figure 7(A)). The discrepancies between the
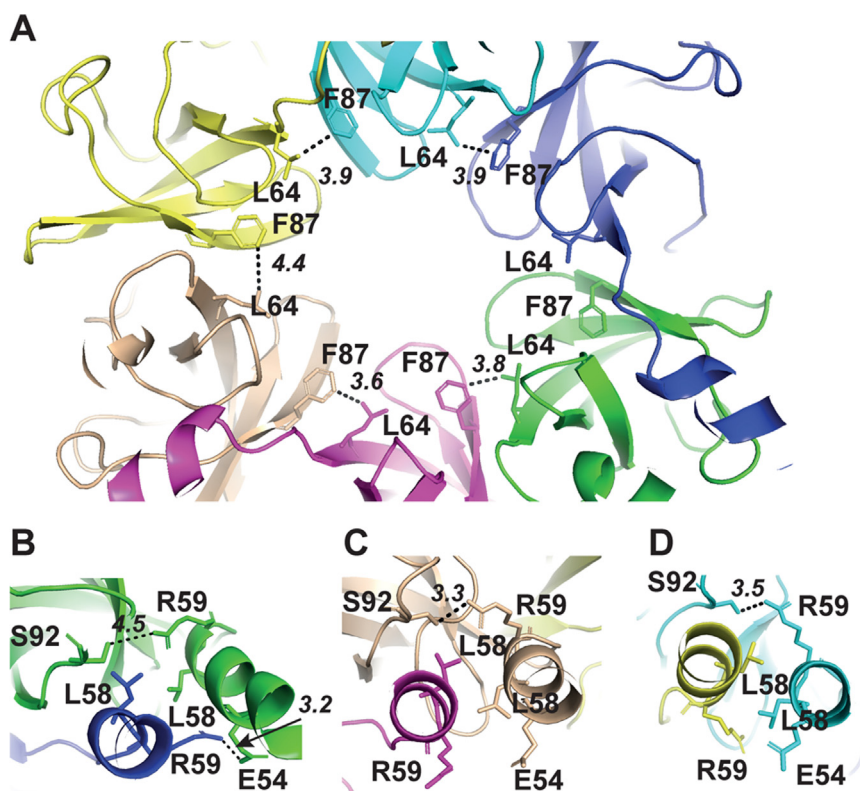
Figure 6. Chemical environment of residues with multiple NMR signals in the EM-derived structure of the homologue protein *Af* PAN. (A) Local structures around residue L64 (corresponding to *Mj* I93) at the six inter-protomer interfaces of *Af* PAN. Also shown is F87, which contacts L64 from the neighbouring protomer, with inter-residue distances given in Å. The protomers are in different colors. (B)–(D) Local structures around residues L58 (corresponding to *Mj* M87) in the three coiled-coil dimers of *Af* PAN, color-coded by protomer. Amino-acids with side-chains at distances of less than ∼4 Å from L58 are shown in sticks. The distances between the side-chains of R59 and S92 are given in Å. The figure was made using the structure from PDB entry 6he8.

NMR data and the cryo-EM structures observed for *Mj* M295 and Mj M159 cannot be explained by the low-resolution of the EM structures, as the EM structures show large differences at protomer interfaces that are not in agreement with C_2 symmetry. Thus, we conclude that the architecture adopted by hexameric PAN in solution and in the absence of substrate is different from the spiral staircase architecture of the cryo-EM structures solved in the presence of substrate.

Finally, the cryo-EM structure of *Af* PAN does not predict the presence of two or three peaks for *Mj* PAN I266, I267, M301, I368, M371, M401 and M412 in solution. For I368, M371, M401 and M412, the local structural environments at the corresponding residues of *Af* PAN (L339, I342, M372 and L383) are very similar across all six protomers (Figure S5(B)). In the context of hexameric *Af* PAN, all these residues have only intra-protomer contacts. Of these four residues only *Af* PAN L383 occupies slightly different environments in the six subunits due to the different conformations of the C-terminal end of the last PAN helix (Figure S5(B)). The two peaks

corresponding to *Mj* M301 (equivalent to *Af* L272) have a volume-ratio of 2:1, which, as explained above, is consistent with C_2 symmetry. Conversely, the local structures of *Af* PAN L272 in the six protomers are only slightly different with no evidence of C_2 symmetry (Figure S5(A)). Similarly, the NMR spectrum indicates that I266 and I267 each experience three environments, with the position of one of the three peaks clearly separated from the other two. In contrast, the local structures at the equivalent residues I237 and I238 of *Af* PAN are only slightly different from each other (Figure S5(C) and (D)) and again there is no evidence of C_2 symmetry. M301, I266 and I267 belong to pore helix α6 and strand β9 on one side of the nucleotide binding pocket and the corresponding residues in *Af* PAN have only intra-protomer contacts. The positional distribution of the NMR peaks of the six copies of each of these residues in the solution NMR spectrum of *Mj* PAN (three peaks, two with either similar or indistinguishable chemical shifts and one with different chemical shift) suggests that the packing-geometries of helix α6 against the central β-sheet
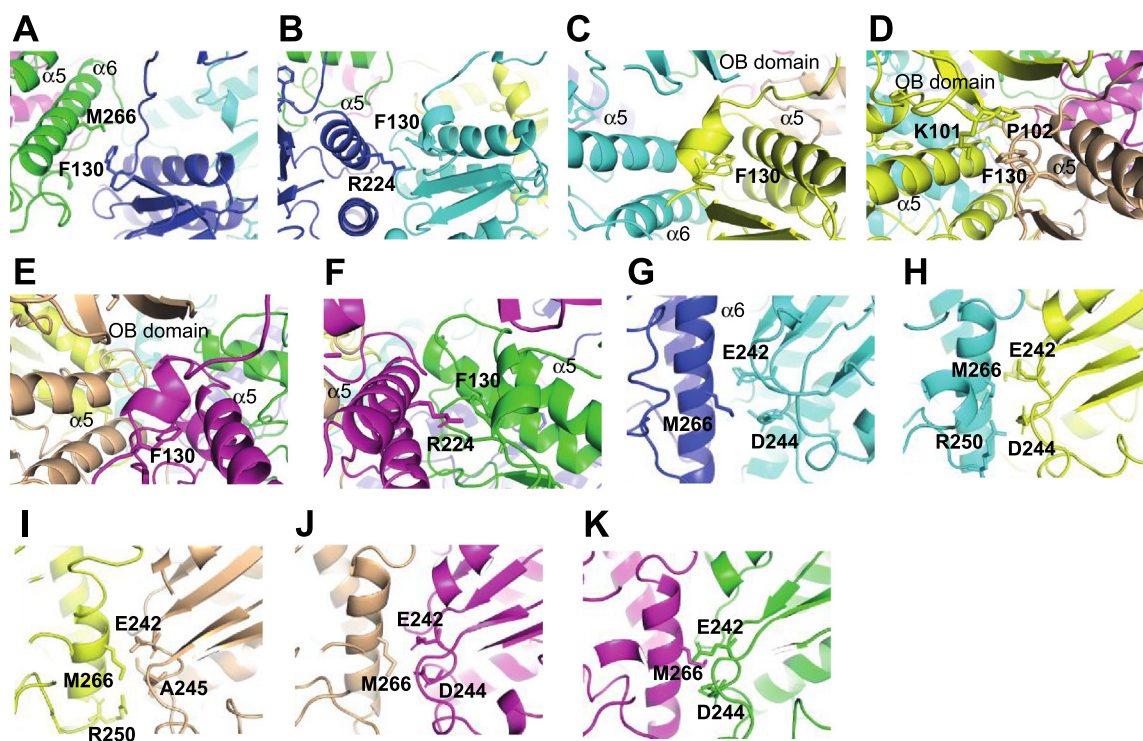
Figure 7. Chemical environment of residues with multiple NMR signals in the EM-derived structure of the homologue protein *Af* PAN. (A)–(F) Local structure around residue F130 (corresponding to *Mj* M159) in all six protomers of *Af* PAN, color-coded by protomer. Amino-acids with side-chains at distances of less than ~4 Å from F130 (and not belonging to the same secondary-structure element as F130) are shown in sticks. (G)–(K) Local structure around residues M266 (corresponding to *Mj* M295) in five protomers of *Af* PAN, color-coded by protomer. The sixth protomer is shown in panel A. Amino-acids with side-chains at distances of less than ~4 Å from M266 (and not belonging to the same secondary-structure element as M266) are shown in sticks. The figure was made using the structure from PDB entry 6he8.

of the ATPase domain are pairwise identical and that, furthermore, are similar in two of the three pairs (corresponding to the peaks at similar positions), but quite different in the third pair (corresponding to the peak with distinct position). It is tempting to correlate this pattern in the disposition of the three peaks with the geometries of the nucleotide binding pockets and their occupancy. Biochemical studies have demonstrated the existence of three types of nucleotide binding pocket, each with different affinity for nucleotides.[26,27] In addition, the cryo-EM structures of *Af* PAN also reveal three distinct binding-pocket geometries, differing in particular in the conformation of the pore-2 loop that comprises the conserved D273-G274-F275 motif following L272 on helix α6 (M301 in *Mj* PAN). Thus, although the cryo-EM structures do not reveal any differences in the local environments of I266, I267 and M301 (probably because of the low resolution), the existence of three different binding-pocket geometries is consistent with both the solution NMR and cryo-EM data.

In summary, the *Af* PAN structures either do not support or are in contradiction with the C_2 symmetry observed in the NMR spectra, leading to the conclusion that the cryo-EM study and this NMR study describe two different states of the enzyme.

The CC and OB domains of PAN do not interact with the degradation signal-peptide. The mechanism by which proteins are targeted to archaeal proteolytic machinery is poorly understood. The bacterial signal-peptide ssrA (AANDENYALAA) functions as a degradation signal in combination with archaeal PAN *in vitro*. Fuzzy interactions between the degradation tag and the N-terminal domains of PAN could act to increase the local substrate concentration at the entrance to the central channel of the ATPase ring, thus initiating unfolding and translocation to the proteolytic core-particle. Hence, we tested whether ssrA interacts with either of the CC or OB domains. The $^1H,^{15}N$ correlation spectra of 300 μM of either dimeric PAN$^{1-89}$ or hexameric PAN$^{74-150}$ in the presence of 3 or 1.9 mM ssrA

peptide showed no change in the chemical shifts of the individual peaks (Figure S6), thus refuting the hypothesis that the CC or OB domains may function to recruit the substrate through recognition of the degradation tag.

An alternative mechanism could involve the hydrophobic ssrA peptide interacting directly with residues in pore-loop 1 of the ATPase domain: in this scenario, when PAN starts pulling on the tag as a consequence of ATP hydrolysis, the stable β-barrel of GFP (or globular core of another substrate protein) would collapse due to steric clashes with the rigid OB-ring.[37] To test this second hypothesis, we added 200 μM of GFP-ssrA to 20 μM of FL PAN hexamer in the presence of 50 mM ADP; no changes were observed in the ^{1}H,^{13}C-HMQC spectrum of the IM-labelled FL PAN (Figure S6). Knowing that ATP increases the affinity of PAN for the substrate,[26] we repeated the experiment in the presence of ATP. However, under these conditions, PAN hydrolysed ATP much faster than in the absence of substrate[39] and had converted the added ATP almost entirely to ADP in the first 30 minutes of the NMR measurement. Thus, we were unable to determine whether pore-loop-1 residues of the ATPase domains of FL PAN are the initial recognition site for GFP-ssrA in the presence of ATP.

Discussion

The presence of three protomer conformations in the PAN unfoldase cannot be easily reconciled with the cryo-EM structures showing five of the six protomers arranged in a spiral staircase. In contrast, the C_2 symmetry seen in the NMR spectra agrees with the existence of three distinct nucleotide-binding-pockets, with high, low and negligible affinity for the nucleotide.[17,26,27] Because the symmetry properties of PAN detected in the NMR spectra extend from the C-terminal tip of the coiled-coil domains to the OB and ATPase domains, it is tempting to posit that the conformations of the nucleotide binding sites are allosterically coupled to those of the CC domains, a situation that would be in agreement with the work of Wilson et al.,[40] who showed that truncation of the first 73 amino acids of the CC domain of *Mj* PAN results in an active PAN variant, which, however, has lost selectivity for ATP and can also bind other nucleotides. Long-range allosteric regulation of substrate processing by the lid of the RP via its CC domains has also been proposed for the human proteasome.[11]

In contrast to the cryo-EM study,[17] our NMR study was conducted in the absence of both the substrate and the core-particle, and in the presence of ADP rather than ATPγS. Thus, it is worth asking whether these differences in the sample composition could be responsible for the observed differences in the symmetry of the unfolding machinery. The NMR

spectra did not change upon addition of ATP, demonstrating that the identity of the nucleotide does not influence the C_2 symmetry of the particle in solution. Interestingly, C_2 symmetry was also observed in a cryo-EM study of the *E. coli* AAA+ ATPase RavA, as an alternative conformation to the spiral staircase.[41] In this work, the ATPase ring in isolation (i.e. not coupled to any other enzyme) was found in two main conformations: a spiral staircase with one large "seam" (corresponding to the gap between the lowest and highest subunits) and five bound nucleotides, and a flat ring with C_2 symmetry, two smaller seams on opposite sides of the ring and four bound nucleotides. This second conformation would be in very good agreement with the symmetry observed in the NMR spectra of *Mj* PAN. A similar pseudo-C_2 symmetry was observed also in the X-ray structure of the ClpX ring.[42]

The C_2 symmetry seen for the *Mj* PAN in solution also has similarities with the AAA+ ATPase ring of the human proteasome in the open-gate state, where the RP channel leading to the CP is open.[43] In this state, the AAA+ ring is arranged in a circle-on-a-saddle topology (referred to as S_{D2} by the authors) with the highest position relative to the CP adopted by the two ATPase subunits on the opposite sides of the ring and only four bound nucleotide molecules.[43] In this topology, the differences in the vertical position of the subunits are much less than in the staircase arrangement, approximating the flat ring seen for RavA. In this study,[43] Zhu et al. propose that binding of six nucleotide molecules to the eukaryotic proteasome stabilizes the resting-state arrangement, while in an actively translocating proteasome the circle-on-a-saddle topology (S_{D2}) with four bound nucleotides becomes predominant. Thus, we conclude that the C_2 symmetry observed for *Mj* PAN in our study represents a common topology of AAA+ ATPase rings.

The differences between the C_2-symmetric arrangement of *Mj* PAN seen in this NMR study and the spiral staircase arrangement seen in cryo-EM studies could be explained by the absence of both substrate and proteasomal particle in the NMR studies. The C_2-symmetric arrangement could represent a nucleotide-bound, resting state of archaeal PAN. The prevalence of the C_2-symmetric conformation in the absence of substrate could explain why the association with PAN with its cognate CP particle requires the substrate: it may act to induce the spiral staircase conformation that is competent for CP binding.

Conclusions

The functional mechanisms of many molecular machines are based on conformational changes, either at the local or global level. Here we demonstrate the relevance of NMR spectroscopy in solution to reveal the conformational properties

of high molecular-weight machinery. Despite the fact that at high molecular-weight solution-state NMR spectroscopy cannot be used to determine full, *de novo* structures, its capability to reveal the three-dimensional environment of specific side-chains at high-resolution and in the entire ensemble of conformations is powerful and unique. Because each NMR signal can be interpreted independently of the others, NMR spectroscopy can focus on selected amino acids in particles that are neither engineered nor selected to favour the most stable conformation. Here, solution-state NMR spectroscopy reveals C_2 symmetry of the AAA+ ATPase ring of PAN in the absence of substrate but in the presence of nucleotide, which likely represents a resting state of PAN.

Materials and methods

Protein expression

All sub-cloning of expression constructs was carried out using a restriction-free cloning approach.[44] Point mutations were introduced following the QuikChange (Agilent Technology) approach. All constructs were confirmed by DNA sequencing.

The GFP-ssrA protein used in this study is a folding-reporter GFP variant.[45] A synthetic gene (GeneCust Europe) of monomeric GFPuv with a C-terminal ssrA tag (AANDENYALAA) and the point mutation A206K[46] was cloned into the pETM11 expression vector (EMBL collection) with an N-terminal His$_6$ purification tag followed by a TEV (tobacco etch virus) protease cleavage-site. The two mutations F64L and S65T were also introduced to yield a folding-reporter GFP variant with improved expression-yields and enhanced stability when expressed in M9 minimal medium for NMR studies.

The synthetic codon-optimized gene (GeneCust Europe) of *Methanocaldoccus jannaschii* PAN was cloned into the pET30a expression-vector carrying a C-terminal His$_6$ purification tag. For proteolysis studies, where PAN must bind the 20S CP and thus requires an accessible C-terminal HbYX-motif, the unfoldase was cloned into a pETM22 expression-vector (EMBL collection), coding for an N-terminal thioredoxin solubility tag (Trx), a His$_6$ purification tag and a 3C-cleavage site. PAN subdomains (CC: residues 1–89; OB-ring: residues 74–150; ATPase-domain: 150–430) were cloned into the pETM22 expression vector.

M. jannaschii 20S proteasome core particle α- and β-subunits were ordered as codon-optimized synthetic genes (GeneCust Europe) and cloned into pET28a and pET30a expression vectors, respectively. The α-subunit carried an N-terminal His$_6$-tag, while the β-subunit, including the six-residue N-terminal pro-peptide, was untagged.

All proteins were expressed in *E. coli* BL21 (DE3) cells and all media contained 50 μg/ml kanamycin (Carl Roth). To produce GFP-ssrA, an overnight culture in lysogeny broth (LB, 50 μg/ml kanamycin) was inoculated from freshly transformed *E. coli* BL21 (DE3) cells on agar plates and incubated at 37 °C overnight. The next day, the main LB culture was inoculated 1:100 and cells were grown at 37 °C to an OD$_{600}$ of 0.8. Next, cells were cooled to 20 °C and expression of GFP-ssrA induced by the addition of 0.1 mM isopropyl-β-D-thio-galactoside (IPTG, Carl Roth). After further incubation at 20 °C for 8 h, expression was stopped and cells were harvested by centrifugation (5000 *g* at 4 °C for 20 min), washed with ice-cold phosphate-buffered saline (PBS) and stored at −80 °C until further use. Cells were resuspended in lysis buffer (50 mM Tris-HCl pH 7.5, 100 mM NaCl, 10 mM imidazole, 5 mM β-mercaptoethanol) supplemented with DNAse I (Roche), complete EDTA-free protease inhibitors (Roche), lysozyme (Carl Roth) and 20 mM MgSO$_4$. After enzymatic lysis for 20 min, cells were disrupted by sonication. Next, the cell debris was removed by centrifugation (19000 *g*, 4 °C, 1 h) and the cleared lysate was loaded onto a 5 ml HisTrap HP IMAC column (Cytiva). Unbound protein was removed by washing with 20 column volumes (CV) of lysis buffer and His$_6$-protein was eluted with 500 mM imidazole in lysis buffer. The N-terminal His$_6$-tag was cleaved overnight with TEV-protease while dialysing the protein against lysis buffer to remove imidazole. The next day, the tag and uncleaved His$_6$-protein were removed by passing the cleavage mix over the HisTrap column. The flow-through containing GFP-ssrA was concentrated using a 10-kDa MWCO Amicon centrifugal filter unit (Millipore) and further purified by gel filtration on a HiLoad 16/600 Superdex S75 pg column (Cytiva) in storage buffer (20 mM Tris-HCl pH 7.5, 100 mM NaCl). Purity and integrity of GFP-ssrA was confirmed by ESI mass spectrometry and the purified protein was concentrated, aliquoted and stored at −80 °C until further use.

Full-length PAN (FL PAN) was produced in two variants, one with a C-terminal uncleavable His$_6$-tag (PAN-His$_6$) and one with an N-terminal Trx-His$_6$-tag (Trx-PAN). For expression of both variants, overnight pre-cultures in LB were inoculated from freshly transformed *E. coli* BL21 (DE3) cells carrying the respective plasmid and incubated for 14–18 h at 37 °C. The main LB cultures were inoculated 1:100 on the next day and cells were grown to an OD$_{600}$ of 0.75. After cooling to 20 °C, expression of PAN was induced by the addition of IPTG (1 mM for PAN-His$_6$, 0.1 mM for Trx-PAN) and cells were incubated at 20 °C for a further 18 h. Cells were harvested by centrifugation (5000 *g* at 4 °C, 20 min), washed with PBS and stored at −80 °C until further use.

Cells producing Trx-PAN were resuspended in lysis-buffer A (20 mM Tris-HCl pH 7.5, 500 mM NaCl, 10 mM MgCl$_2$, 10 mM imidazole and 5 mM β-mercaptoethanol) supplemented with DNAse I (Roche), RNAse (Roche), complete EDTA-free protease inhibitor cocktail (Roche) and lysozyme. After enzymatic lysis for 20 min, cells were disrupted by sonication. Next, the cell debris was removed by centrifugation (19000 *g*, 4 °C, 1 h) and the cleared lysate was loaded onto a 5 ml HisTrap HP IMAC column (Cytiva). Unbound protein was washed from the column with lysis buffer A. The Trx-PAN protein was eluted with a gradient of 50–500 mM imidazole in 10 CVs, and peak-fractions were exchanged into lysis buffer using a HiPrep 26/10 desalting column. The Trx-His$_6$-tag was cleaved with 3C protease overnight. The cleavage mix was purified with a HisTrap column. Cleaved PAN was buffer-exchanged to the storage buffer (20 mM Tris-HCl pH 7.5, 100 mM NaCl, 10 mM MgCl$_2$). Cells producing PAN-His$_6$ were lysed in the PAN-storage buffer supplemented with 5 mM imidazole, DNAse I (Roche), RNAse (Roche), lysozyme, complete EDTA-free protease inhibitor cocktail (Roche), 1 mg/ml AEBSF protease inhibitor and 0.1 % (v/v) Triton X-100 (Sigma Aldrich), lysed and centrifuged as for the Trx-PAN construct. The cleared lysate was loaded onto a Histrap HP IMAC column. Unbound protein was washed with 10 CVs of 25 mM imidazole and 10 CVs of 50 mM imidazole in PAN storage buffer, before PAN-His$_6$ was eluted with 500 mM imidazole. Imidazole was removed by buffer-exchange into the storage buffer. Both cleaved PAN from Trx-PAN and PAN-His$_6$ were further purified by anion exchange chromatography on a 5 ml HiTrap Q HP column. Finally, PAN and PAN-His$_6$ were purified on a HiLoad 16/600 Superdex 200 pg size exclusion chromatography (SEC) column in storage buffer, concentrated using a 100-kDa MWCO Amicon centrifugal filter (Millipore) and stored at –80 °C.

Cells containing the pETM22-Trx-PAN-CC plasmid (expressing PAN$^{1-89}$) were lysed in lysis buffer, purified and cleaved as for Trx-PAN. Cleaved PAN$^{1-89}$ was separated from the cleavage mix via a second round of affinity chromatography. After concentration, PAN$^{1-89}$ was further purified by SEC on a HiLoad 16/600 Superdex 200 pg column in CC-buffer (20 mM MES pH 6.5, 100 mM NaCl, 10 mM MgCl$_2$, 0.1 % NaN$_3$). The pure protein was concentrated and frozen at –80 °C until further use.

Cells expressing the pETM22-Trx-PAN-OB-ring plasmid (coding for PAN$^{74-150}$) were lysed in lysis buffer, purified and cleaved as for Trx-PAN; however, in this case the buffer consisted of HEPES at pH 7.0. After cleavage, PAN$^{74-150}$ was buffer-exchanged to the cation-exchange buffer (20 mM HEPES, 100 mM NaCl, 10 mM MgCl$_2$, pH 7.0) and purified on a SP FF cation exchange column (Cytiva). Finally, PAN$^{74-150}$ was purified by SEC with a Superdex 200 increase 10/300 GL column (Cytiva) in PAN-storage buffer, concentrated and stored at –80 °C until further use.

PAN$^{150-430}$ was expressed with the F196A point mutation for improved solubility. In addition, the construct used for NMR assignment also incorporated the five mutations K406S, K414–416E and K418E, which were designed to eliminate basic charges on one face of the ATPase-domain hexameric ring and thereby hinder formation of higher-order aggregates. This mutant variant of PAN$^{150-430}$ was expressed and purified in the same way as PAN from the Trx-PAN fusion construct, as described above. The final SEC was carried out on a HiLoad 16/600 Superdex 75 pg column in ATPase-domain storage buffer (20 mM MES, 500 mM NaCl, 10 mM MgCl$_2$, 2 mM TCEP, pH 6.1).

The *M. jannaschii* 20S proteasome was assembled from the individual domains following the protocol previously reported for the *T. acidophilum* 20S CP.[47] Individual subunits were expressed separately. Freshly transformed *E. coli* BL21 (DE3) cells harbouring either the pET28a-20S-α-subunit or the pET30a-20Sβ-subunit plasmids were used to inoculate an LB overnight culture (50 µg/ml kanamycin). The next day, the main LB culture was prepared by inoculating 1:100 from the overnight culture and grown at 37 °C to an OD$_{600}$ of 0.8. Cells were cooled to room temperature and proteins were expressed by addition of 1 mM IPTG, followed by incubation at 20 °C for 18 h. Cells were harvested by centrifugation (5000 *g* at 4 °C, 20 min), washed with PBS and stored at –80 °C until further use.

Cells expressing the α-subunits were resuspended in lysis buffer (20 mM Tris-HCl pH 7.5, 100 mM NaCl, 10 mM MgCl$_2$, 5 mM imidazole), supplemented with complete EDTA-free protease inhibitor cocktail (Roche), DNAse I (Roche), lysozyme (Carl Roth, Germany), incubated at room temperature for 15 min and lysed by sonication. The cell debris was removed by centrifugation at 19000 *g* and 4 °C for 1 h. The cleared lysate was loaded onto a HisTrap HP 5 ml column (Cytiva) pre-equilibrated in lysis buffer. Unbound protein was washed from the column with 10 CVs of lysis buffer. 20S-α-subunits were eluted with 500 mM imidazole in lysis buffer and then buffer-exchanged into storage buffer (20 mM Tris-HCl pH 7.5, 100 mM NaCl, 10 mM MgCl$_2$) with a HiPrep 26/10 desalting column (Cytiva). The α-subunits were further purified by anion-exchange chromatography on a HiTrap Q HP 5 ml column (Cytiva) with elution over a gradient of 100–500 mM NaCl in 10 CVs. Finally, the protein was concentrated (Amicon 15, 10-kDa MWCO, Millipore) and further purified by SEC with a HiLoad 16/600 Superdex 200 pg column in storage buffer. The fractions corresponding to

single heptameric α-rings were collected and kept at 4 °C until assembly of the 20S.

Cells expressing the β-subunits were resuspended in storage buffer, supplemented with protease inhibitors, DNAse and lysozyme, incubated at room temperature for 15 min and lysed by two passages through a high-pressure homogenizer (Avestin Emulsiflex C5, 15000 psi). The lysate was cleared by centrifugation (19000 g at 4 °C for 1 h) and loaded onto a 5 ml HiTrap SP HP cation exchange column (GE Healthcare) pre-equilibrated in storage buffer. Unbound protein was removed by washing with 10 CVs of storage buffer; the bound protein was eluted with a gradient of 100–1000 mM NaCl in 20 CVs. β-subunits were concentrated (Amicon-15, 10-kDa MWCO, Millipore) and further purified by SEC with a HiLoad 16/600 Superdex 75 pg column in storage buffer.

The 20S CP was assembled by mixing purified but not concentrated β-subunits with α-rings, gently shaking at 37 °C (volume ≈ 30 ml). 0.02 % NaN$_3$ (Sigma Aldrich) was added to prevent microbial growth. After 6 h, the mix was concentrated to 2 ml (Amicon-15, 100-kDa MWCO, Millipore) at ambient temperature and further incubated at 37 °C for 16 h. Finally, the assembled 20S proteasome was purified by SEC with a HiLoad 16/600 Superdex 200 pg column in storage buffer. Fractions corresponding to the α$_7$β$_7$β$_7$α$_7$ particle were collected, concentrated and stored at –80 °C until further use. Pro-peptide auto-catalysis of the β-subunits was confirmed by ESI-mass spectrometry.

Isotopic labelling and deuteration

Production of isotopically enriched proteins was carried out in M9 minimal medium. Uniformly ^{13}C,^{15}N-labelled proteins (GFP-ssrA, PAN$^{1−89}$) were expressed in M9 minimal medium containing 1 g/l ^{15}NH$_4$CL and 4 g/l ^{13}C-D-glucose (Eurisotop and Sigma Aldrich). All deuterated proteins (PAN$^{74−150}$, PAN$^{150−430}$, full-length PAN) were produced in minimal medium containing 99% D$_2$O. 99% deuteration was achieved using 4 g/l deuterated carbon sources (^{2}H$_7$-D-glucose, ^{2}H$_8$-glycerol, Eurisotop). Deuterated protein samples for backbone assignment experiments were prepared using D$_2$O-based minimal medium containing 1 g/l ^{15}NH$_4$Cl and 4 g/l [^{13}C$_6$;^{2}H$_7$]-D-glucose (Eurisotop). Deuterated ILV-methyl-^{1}H,^{13}C-labelled proteins were produced by the addition of appropriately labelled α-ketoacid amino-acid precursors to the cell culture 1 h before induction with IPTG.[48] For side-chain assignment, the following labelling scheme was adopted, yielding full ^{13}C-labelling of the side-chain: [^{13}C$_4$,3,3-^{2}H$_2$]-α-ketobutyrate (60 mg/l) and [1,2,3,4-^{13}C$_4$; 3,4′,4′,4′-^{2}H$_4$]-α-ketoisovalerate acid (120 mg/ml) (Eurisotop and Sigma Aldrich). For NOESY-based experiments (PAN$^{150−430}$) and for

full-length PAN [methyl-^{13}C;3,3-^{2}H$_2$] α-ketobutyrate (methyl-^{13}C, 99%; 3,3-D2, 98%) and [3-methyl-^{13}C; 3,4,4,4-^{2}H$_4$]-α-ketoisovalerate were added instead (Eurisotop and Sigma Aldrich). ^{1}H,^{13}C-labelling of Met-ε methyl groups in deuterated proteins was achieved by adding the SLAM-methionine labelling kit (NMR-Bio) 30 min before the addition of ILV precursors. Isotopically labelled and deuterated proteins were purified identically to the unlabelled proteins.

SEC-MALS

SEC-MALS (SEC, size-exclusion-chromatography; MALS, multiple-angle-light-scattering) experiments were carried out using either a Superdex 200 increase 10/300 GL column in PAN-storage buffer (PAN$^{150−430}$, PAN$^{74−150}$) or a Superdex 75 increase 10/300 GL column in coiled-coil buffer (PAN$^{1−89}$) or a Superose 6 increase, 10/300 GL (FL PAN), all from Cytiva. Light-scattering and refractivity-index values were obtained from mini-DAWN TREOS and Optilab T-rEX detectors, respectively (both from Wyatt). The molecular weights were calculated with the software ASTRA 7 (Wyatt).

Fluorescence measurements of GFP-ssrA unfolding and degradation

Unfolding and degradation of GFP-ssrA by PAN and PAN–20S was carried out in a StepOne RT-PCR system (Thermo Scientific) monitoring intrinsic GFP fluorescence with ROX-dye filters to prevent detector saturation. The buffer was 20 mM Tris-HCl, pH 7.5, 100 mM NaCl, 100 mM MgCl$_2$ (Sigma Aldrich) and 100 mM ATP (Carl Roth). 100 μM GFP-ssrA in buffer was incubated either with 5 μM PAN alone or with 5 μM PAN and 5 μM 20S in a final volume of 25 μl and fluorescence was measured at 60 °C in 10 s intervals. All runs were repeated in triplicate.

NMR experiments

All NMR spectra were recorded on Bruker Avance III HD 600-MHz (resonance assignment experiments) and 850-MHz (resonance assignments and time-course experiments) spectrometers running TopSpin 3.2 software and equipped with N$_2$-cooled and He-cooled inverse HCN triple-resonance cryogenic probes, respectively. Spectra were processed with TopSpin 3.2 (time-course experiments) or NMRPipe[49] (all other experiments) and analysed in CcpNmr Analysis v2.4.[50]

Resonance assignments

PAN CC. Backbone resonance assignment experiments of the PAN$^{1−89}$ were recorded on 1 mM (monomer) U- [^{15}N, ^{13}C] labelled protein in 20 mM MES pH 6.5, 100 mM NaCl, 10 mM MgCl$_2$,

0.1 % NaN$_3$, 10 % D$_2$O and included 2D ^{15}N-HSQC,[51,52] 3D HNCO, 3D HN(CO)CACB and 3D HNCACB, 3D HN(CO)CA and 3D HNCA[53–58] at 45 °C.

PAN OB-ring. Backbone resonance assignment experiments of PAN$^{74–150}$ were recorded on U-[^{2}H, ^{13}C, ^{15}N]-labelled protein as a set of TROSY-based experiments (^{1}H,^{15}N-TROSY-HSQC, 3D TROSY-HNCO, 3D TROSY-HN(CA)CO, 3D TROSY-HNCA, 3D HN(CO)CA, 3D TROSY HN(COCA)CB, 3D TROSY-HNCACB, 3D TROSY HN(CA)CB).[59–61] Samples were prepared at 600–700 µM monomer (100–120 µM PAN OB-ring hexamer) in NMR buffer (20 mM Tris-HCl, 100 mM NaCl, 10 mM MgCl$_2$, 0.05 % NaN$_3$, pH 7.5, 10 % D$_2$O). Assignment of ILV-methyl resonances was achieved via an HMCM[CG]-CBCA COSY experiment,[48] measured on triple-labelled samples [^{2}H, ^{13}C, ^{15}N], where Ile-δ1-, Leu-δ, Val-γ methyl groups were selectively protonated. All experiments were conducted at 60 °C.

PAN ATPase-domain. Backbone assignment of PAN$^{150–430}$ was conducted on the monomeric mono-disperse F196A mutant construct. A further five C-terminal point mutations were included, which reduce the formation of dodecamers in full-length PAN (K406S, K414E, K415E, K416E, K418E). The set of assignment experiments was recorded on 600 µM U-[^{2}H, ^{13}C, ^{15}N]-labelled samples in 20 mM MES, 500 mM NaCl, 10 mM MgCl$_2$, 2 mM TCEP, 0.05 % NaN$_3$, pH 6.1, 10% D$_2$O, and consisted of ^{1}H,^{15}N-TROSY-HSQC, 3D TROSY-HNCO and 3D TROSY-HNCACB spectra. Resonance assignments of Ile-δ1-, Leu-δ, Val-γ methyl groups were obtained via the HMCM[CG]-CBCA COSY experiment, recorded on U-[^{2}H, ^{13}C, ^{15}N]-labelled samples with selective protonation of the respective methyl groups. Methionine-ε-methyl groups were assigned using inter-methyl NOEs obtained from a 3D ^{13}C-HMQC–NOESY–^{13}C-HMQC spectrum[62,63] recorded on a PAN$^{150–430}$ sample that was uniformly ^{2}H,^{15}N-labelled, with the exception of Ile-δ1-, Leu-δ, Val-γ and Met- ε-methyl groups, which were ^{1}H,^{13}C-labelled. Experimental NOEs were compared to those predicted from the PDB entry 3H4M.[32] In total 8 out of 9 Met-ε, 22 out of 24 Ile-δ1, 41 out of 50 Leu-δ and 40 out of 40 Val-γ methyl-resonances were assigned unambiguously. The Leu and Val methyl-group assignments were non-stereospecific. All experiments on the PAN$^{150–430}$ construct were conducted at 60 °C.

Full-length PAN. Ile-δ1 and Met-ε methyl-group assignments of PAN$^{150–430}$ were transferred to the full-length protein by overlaying the ^{1}H,^{13}C-HSQC spectrum of PAN$^{150–430}$ with the ^{1}H,^{13}C-HMQC[34] spectrum of 20 µM full-length PAN hexamer in 20 mM Tris-HCl, 100 mM NaCl, 10 mM MgCl$_2$ pH 7.5 in 100 % D$_2$O and in the presence of 50 mM ADP. Likewise, we transferred the assignment of the two Ile methyl groups from PAN$^{74–150}$. The assignments of the Met-ε methyl groups of PAN$^{1–89}$ and PAN$^{74–150}$, as well as the assignments of the Ile-δ1 methyl groups of PAN$^{1–89}$ were obtained by point-mutations. All spectra of FL PAN were recorded at 60 °C on the 850-MHz spectrometer.

Backbone dynamics of PAN$^{1–89}$

Backbone dynamics of the homodimeric PAN$^{1–89}$ were measured with a set of ^{15}N heteronuclear NOE, ^{15}N-R_1 and ^{15}N-$R_{1\rho}$ relaxation experiments on uniformly ^{15}N-labeled protein (buffer: 20 mM MES, 100 mM NaCl, 10 mM MgCl$_2$, 0.1% NaN$_3$, 10% D$_2$O, pH 6.5).[65–66] To measure R_1, twelve longitudinal recovery delays were chosen in the range 20–1600 ms. To obtain reliable data for both the broad and the sharp ^{15}N-^{1}H peaks, $R_{1\rho}$ experiments were recorded at two ^{15}N-spin-lock-strengths (1.25 kHz and 2.5 kHz), using maximum relaxation delays of 200 and 100 ms, respectively. Pseudo-3D spectra were processed with NMRPipe and integration of peaks was carried out with the line-shape fitting program FuDA (D.F. Hansen, https://www.ucl.ac.uk/hansen-lab/fuda/). Initial estimates of the peak positions and linewidths were obtained using CcpNMR Analysis and used as starting values for the FuDA fitting procedure. Data analysis, including the fitting of peak-volumes to obtain R_1 and $R_{1\rho}$ relaxation rates and the calculation of intensity-ratios for the heteronuclear NOE, was carried out using in-house scripts.

CRediT authorship contribution statement

Acknowledgments

Declaration of Competing Interest

The authors declare that they have no known competing financial interests or personal

relationships that could have appeared to influence the work reported in this paper.

Appendix A. Supplementary Data

Supplementary data to this article can be found online at https://doi.org/10.1016/j.jmb.2023.167997.

References

1. Yedidi, R.S., Wendler, P., Enenkel, C., (2017). AAA-ATPases in Protein Degradation. *Front. Mol. Biosci.* **4**
2. Chen, B., Retzlaff, M., Roos, T., Frydman, J., (2011). Cellular Strategies of Protein Quality Control. *Cold Spring Harb. Perspect. Biol.* **3**
3. Bassermann, F., Eichner, R., Pagano, M., (2014). The ubiquitin proteasome system — Implications for cell cycle control and the targeted treatment of cancer. *Biochimica et Biophysica Acta (BBA) - Molecular Cell Res.* **1843**, 150–162.
4. Majumder, P., Baumeister, W., (2019). Proteasomes: unfoldase-assisted protein degradation machines. *Biol. Chem.* **401**, 183–199.
5. Pickart, C.M., Cohen, R.E., (2004). Proteasomes and their kin: proteases in the machine age. *Nat. Rev. Mol. Cell Biol.* **5**, 177–187.
6. Bard, J.A.M., Goodall, E.A., Greene, E.R., Jonsson, E., Dong, K.C., Martin, A., (2018). Structure and Function of the 26S Proteasome. *Annu. Rev. Biochem.* **87**, 697–724.
7. Humbard, M.A., Maupin-Furlow, J.A., (2013). Prokaryotic proteasomes: nanocompartments of degradation. *J. Mol. Microbiol. Biotechnol.* **23**, 321–334.
8. Maupin-Furlow, J., (2012). Proteasomes and protein conjugation across domains of life. *Nat. Rev. Microbiol.* **10**, 100–111.
9. Berko, D., Tabachnick-Cherny, S., Shental-Bechor, D., Cascio, P., Mioletti, S., Levy, Y., et al., (2012). The Direction of Protein Entry into the Proteasome Determines the Variety of Products and Depends on the Force Needed to Unfold Its Two Termini. *Mol. Cell* **48**, 601–611.
10. de la Peña, A.H., Goodall, E.A., Gates, S.N., Lander, G.C., Martin, A., (2018). Substrate-engaged 26S proteasome structures reveal mechanisms for ATP-hydrolysis–driven translocation. *Science* **362**, eaav0725.
11. Dong, Y., Zhang, S., Wu, Z., Li, X., Wang, W.L., Zhu, Y., et al., (2019). Cryo-EM structures and dynamics of substrate-engaged human 26S proteasome. *Nature* **565**, 49–55.
12. Lander, G.C., Estrin, E., Matyskiela, M.E., Bashore, C., Nogales, E., Martin, A., (2012). Complete subunit architecture of the proteasome regulatory particle. *Nature* **482**, 186–191.
13. Matyskiela, M.E., Lander, G.C., Martin, A., (2013). Conformational switching of the 26S proteasome enables substrate degradation. *Nat. Struct. Mol. Biol.* **20**, 781–788.
14. Sledz, P., Unverdorben, P., Beck, F., Pfeifer, G., Schweitzer, A., Forster, F., et al., (2013). Structure of the 26S proteasome with ATP-gamma S bound provides insights into the mechanism of nucleotide-dependent substrate translocation. *PNAS* **110**, 7264–7269.
15. Huang, X., Luan, B., Wu, J., Shi, Y., (2016). An atomic structure of the human 26S proteasome. *Nat. Struct. Mol. Biol.* **23**, 778–785.
16. Unverdorben, P., Beck, F., Sledz, P., Schweitzer, A., Pfeifer, G., Plitzko, J.M., et al., (2014). Deep classification of a large cryo-EM dataset defines the conformational landscape of the 26S proteasome. *PNAS* **111**, 5544–5549.
17. Majumder, P., Rudack, T., Beck, F., Danev, R., Pfeifer, G., Nagy, I., et al., (2019). Cryo-EM structures of the archaeal PAN-proteasome reveal an around-the-ring ATPase cycle. *PNAS* **116**, 534–539.
18. Tsai, F.T.F., Hill, C.P., (2020). Same structure, different mechanisms? *Elife* **9**, e56501.
19. Fei, X., Bell, T.A., Jenni, S., Stinson, B.M., Baker, T.A., Harrison, S.C., et al., (2020). Structures of the ATP-fueled ClpXP proteolytic machine bound to protein substrate. *Elife* **9**, e52774.
20. Ripstein, Z.A., Vahidi, S., Houry, W.A., Rubinstein, J.L., Kay, L.E., (2020). A processive rotary mechanism couples substrate unfolding and proteolysis in the ClpXP degradation machinery. *Elife* **9**
21. Maillard, R.A., Chistol, G., Sen, M., Righini, M., Tan, J., Kaiser, C.M., et al., (2011). ClpX(P) generates mechanical force to unfold and translocate its protein substrates. *Cell* **145**, 459–469.
22. Aubin-Tam, M.E., Olivares, A.O., Sauer, R.T., Baker, T.A., Lang, M.J., (2011). Single-molecule protein unfolding and translocation by an ATP-fueled proteolytic machine. *Cell* **145**, 257–267.
23. Cordova, J.C., Olivares, A.O., Shin, Y., Stinson, B.M., Calmat, S., Schmitz, K.R., et al., (2014). Stochastic but highly coordinated protein unfolding and translocation by the ClpXP proteolytic machine. *Cell* **158**, 647–658.
24. Sen, M., Maillard, R.A., Nyquist, K., Rodriguez-Aliaga, P., Presse, S., Martin, A., et al., (2013). The ClpXP protease unfolds substrates using a constant rate of pulling but different gears. *Cell* **155**, 636–646.
25. Martin, A., Baker, T.A., Sauer, R.T., (2005). Rebuilt AAA plus motors reveal operating principles for ATP-fuelled machines. *Nature* **437**, 1115–1120.
26. Smith, D.M., Fraga, H., Reis, C., Kafri, G., Goldberg, A.L., (2011). ATP binds to proteasomal ATPases in pairs with distinct functional effects, implying an ordered reaction cycle. *Cell* **144**, 526–538.
27. Stinson, B.M., Nager, A.R., Glynn, S.E., Schmitz, K.R., Baker, T.A., Sauer, R.T., (2013). Nucleotide binding and conformational switching in the hexameric ring of a AAA+ machine. *Cell* **153**, 628–639.
28. Hersch, G.L., Burton, R.E., Bolon, D.N., Baker, T.A., Sauer, R.T., (2005). Asymmetric interactions of ATP with

the AAA+ ClpX6 unfoldase: allosteric control of a protein machine. *Cell* **121**, 1017–1027.

29. Yu, Y., Liu, H., Yu, Z., Witkowska, H.E., Cheng, Y., (2020). Stoichiometry of Nucleotide Binding to Proteasome AAA+ ATPase Hexamer Established by Native Mass Spectrometry. *Mol. Cell. Proteomics* **19**, 1997–2015.

30. Lapinaite, A., Simon, B., Skjaerven, L., Rakwalska-Bange, M., Gabel, F., Carlomagno, T., (2013). The structure of the box C/D enzyme reveals regulation of RNA methylation. *Nature* **502**, 519–523.

31. Sprangers, R., Kay, L.E., (2007). Quantitative dynamics and binding studies of the 20S proteasome by NMR. *Nature* **445**, 618–622.

32. Zhang, F., Hu, M., Tian, G., Zhang, P., Finley, D., Jeffrey, P.D., et al., (2009). Structural insights into the regulatory particle of the proteasome from Methanocaldococcus jannaschii. *Mol. Cell* **34**, 473–484.

33. Caillat, C., Macheboeuf, P., Wu, Y., McCarthy, A.A., Boeri-Erba, E., Effantin, G., et al., (2015). Asymmetric ring structure of Vps4 required for ESCRT-III disassembly. *Nat. Commun.* **6**, 8781.

34. Tugarinov, V., Hwang, P.M., Ollerenshaw, J.E., Kay, L.E., (2003). Cross-correlated relaxation enhanced ^{1}H–^{13}C NMR spectroscopy of methyl groups in very high molecular weight proteins and protein complexes. *J. Am. Chem. Soc.* **125**, 10420–10428.

35. Reddy, G., Liu, Z., Thirumalai, D., (2012). Denaturant-dependent folding of GFP. *PNAS* **109**, 17832–17838.

36. Benaroudj, N., Goldberg, A.L., (2000). PAN, the proteasome-activating nucleotidase from archaebacteria, is a protein-unfolding molecular chaperone. *Nat. Cell Biol.* **2**, 833–839.

37. Zhang, F., Wu, Z., Zhang, P., Tian, G., Finley, D., Shi, Y., (2009). Mechanism of substrate unfolding and translocation by the regulatory particle of the proteasome from Methanocaldococcus jannaschii. *Mol. Cell* **34**, 485–496.

38. Djuranovic, S., Hartmann, M.D., Habeck, M., Ursinus, A., Zwickl, P., Martin, J., et al., (2009). Structure and Activity of the N-Terminal Substrate Recognition Domains in Proteasomal ATPases. *Mol. Cell* **34**, 580–590.

39. Benaroudj, N., Zwickl, P., Seemuller, E., Baumeister, W., Goldberg, A.L., (2003). ATP hydrolysis by the proteasome regulatory complex PAN serves multiple functions in protein degradation. *Mol. Cell* **11**, 69–78.

40. Wilson, H.L., Ou, M.S., Aldrich, H.C., Maupin-Furlow, J., (2000). Biochemical and physical properties of the Methanococcus jannaschii 20S proteasome and PAN, a homolog of the ATPase (Rpt) subunits of the eucaryal 26S proteasome. *J. Bacteriol.* **182**, 1680–1692.

41. Jessop, M., Arragain, B., Miras, R., Fraudeau, A., Huard, K., Bacia-Verloop, M., et al., (2020). Structural insights into ATP hydrolysis by the MoxR ATPase RavA and the LdcI-RavA cage-like complex. *Commun Biol.* **3**, 46.

42. Glynn, S.E., Martin, A., Nager, A.R., Baker, T.A., Sauer, R.T., (2009). Structures of asymmetric ClpX hexamers reveal nucleotide-dependent motions in a AAA+ protein-unfolding machine. *Cell* **139**, 744–756.

43. Zhu, Y., Wang, W.L., Yu, D., Ouyang, Q., Lu, Y., Mao, Y., (2018). Structural mechanism for nucleotide-driven remodeling of the AAA-ATPase unfoldase in the activated human 26S proteasome. *Nat. Commun.* **9**, 1360.

44. van den Ent, F., Löwe, J., (2006). RF cloning: A restriction-free method for inserting target genes into plasmids. *J. Biochem. Bioph. Methods* **67**, 67–74.

45. Waldo, G.S., Standish, B.M., Berendzen, J., Terwilliger, T.C., (1999). Rapid protein-folding assay using green fluorescent protein. *Nat. Biotechnol.* **17**, 691–695.

46. Zacharias, D.A., Violin, J.D., Newton, A.C., Tsien, R.Y., (2002). Partitioning of Lipid-Modified Monomeric GFPs into Membrane Microdomains of Live Cells. *Science* **296**, 913–916.

47. Velyvis, A., Ruschak, A.M., Kay, L.E., (2012). An economical method for production of ^{2}H, ^{13}CH$_3$-threonine for solution NMR studies of large protein complexes: application to the 670 kDa proteasome. *PLoS One* **7**, e43725.

48. Tugarinov, V., Kay, L.E., (2003). Ile, Leu, and Val methyl assignments of the 723-residue malate synthase G using a new labeling strategy and novel NMR methods. *J. Am. Chem. Soc.* **125**, 13868–13878.

49. Delaglio, F., Grzesiek, S., Vuister, G.W., Zhu, G., Pfeifer, J., Bax, A., (1995). NMRPipe: A multidimensional spectral processing system based on UNIX pipes. *J. Biomol. NMR* **6**, 277–293.

50. Vranken, W.F., Boucher, W., Stevens, T.J., Fogh, R.H., Pajon, A., Llinas, M., et al., (2005). The CCPN data model for NMR spectroscopy: Development of a software pipeline. *Proteins Struct. Funct. Bioinf.* **59**, 687–696.

51. Bodenhausen, G., Ruben, D., (1980). Natural abundance nitrogen-15 NMR by enhanced heteronuclear spectroscopy. *Chem. Phys. Lett.* **69**, 185–189.

52. Piotto, M., Saudek, V., Sklenar, V., (1992). Gradient-tailored excitation for single-quantum NMR spectroscopy of aqueous solutions. *J. Biomol. NMR* **2**, 661–665.

53. Ikura, M., Kay, L.E., Bax, A., (1990). A novel approach for sequential assignment of ^{1}H, ^{13}C, and ^{15}N spectra of proteins: heteronuclear triple-resonance three-dimensional NMR spectroscopy. Application to calmodulin. *Biochemistry* **29**, 4659–4667.

54. Kay, L.E., Ikura, M., Tschudin, R., Bax, A., (1969). Three-dimensional triple-resonance NMR spectroscopy of isotopically enriched proteins. *J. Magn. Reson.* **1990** (89), 496–514.

55. Bax, A., Ikura, M., (1991). An efficient 3D NMR technique for correlating the proton and ^{15}N backbone amide resonances with the α-carbon of the preceding residue in uniformly ^{15}N/^{13}C enriched proteins. *J. Biomol. NMR* **1**, 99–104.

56. Grzesiek, S., Bax, A., (1969). Improved 3D triple-resonance NMR techniques applied to a 31 kDa protein. *J. Magn. Reson.* **1992** (96), 432–440.

57. Wittekind, M., Mueller, L., (1993). HNCACB, a High-Sensitivity 3D NMR Experiment to Correlate Amide-Proton and Nitrogen Resonances with the Alpha- and Beta-Carbon Resonances in Proteins. *J. Magn. Reson. B* **101**, 201–205.

58. Yamazaki, T., Lee, W., Arrowsmith, C.H., Muhandiram, D.R., Kay, L.E., (1994). A Suite of Triple Resonance NMR Experiments for the Backbone Assignment of ^{15}N, ^{13}C, ^{2}H Labeled Proteins with High Sensitivity. *J. Am. Chem. Soc.* **116**, 11655–11666.

59. Pervushin, K., Riek, R., Wider, G., Wüthrich, K., (1997). Attenuated T_2 relaxation by mutual cancellation of dipole–

dipole coupling and chemical shift anisotropy indicates an avenue to NMR structures of very large biological macromolecules in solution. *Proc. Natl. Acad. Sci.* **94**, 12366.

60. Salzmann, M., Pervushin, K., Wider, G., Senn, H., Wüthrich, K., (1998). TROSY in triple-resonance experiments: New perspectives for sequential NMR assignment of large proteins. *Proc. Natl. Acad. Sci.* **95**, 13585.

61. Salzmann, M., Wider, G., Pervushin, K., Senn, H., Wüthrich, K., (1999). TROSY-type Triple-Resonance Experiments for Sequential NMR Assignments of Large Proteins. *J. Am. Chem. Soc.* **121**, 844–848.

62. Vuister, G.W., Clore, G.M., Gronenborn, A.M., Powers, R., Garrett, D.S., Tschudin, R., et al., (1993). Increased Resolution and Improved Spectral Quality in Four-Dimensional ^{13}C/^{13}C-Separated HMQC-NOESY-HMQC Spectra Using Pulsed Field Gradients. *J. Magn. Reson. B* **101**, 210–213.

63. Clore, G.M., Kay, L.E., Bax, A., Gronenborn, A.M., (1991). Four-dimensional carbon-13/carbon-13-edited nuclear Overhauser enhancement spectroscopy of a protein in solution: application to interleukin 1 beta. *Biochemistry* **30**, 12–18.

64. Kay, L.E., Torchia, D.A., Bax, A., (1989). Backbone dynamics of proteins as studied by nitrogen-15 inverse detected heteronuclear NMR spectroscopy: application to staphylococcal nuclease. *Biochemistry* **28**, 8972–8979.

65. Li, Y.C., Montelione, G.T., (1994). Overcoming Solvent Saturation-Transfer Artifacts in Protein NMR at Neutral pH. Application of Pulsed Field Gradients in Measurements of ^{1}H–^{15}N Overhauser Effects. *J. Magn. Reson. B* **105**, 45–51.

66. Mulder, F.A.A., de Graaf, R.A., Kaptein, R., Boelens, R., (1998). An Off-resonance Rotating Frame Relaxation Experiment for the Investigation of Macromolecular Dynamics Using Adiabatic Rotations. *J. Magn. Reson.* **131**, 351–357.